Magnetic control over the fractal dimension of supramolecular rod networks

Vincent Marichez, Akihiro Sato, Peter Dunne, Jorge Leira-Iglesias, Georges J.M. Formon, Michaela K. Schicho, Isja de Feijter, Pascal Hébraud, Matthieu Bailleul, Pol Besenius, M. Venkatesan, J.M.D. Coey, E.W. Meijer, and Thomas M. Hermans*

Abstract: Controlling supramolecular polymerization is of fundamental importance to create advanced materials and devices. Here we show that the thermodynamic equilibrium of Gd^{3+}-bearing supramolecular rod networks is shifted reversibly at room temperature in a static magnetic field of up to 2 T. Our approach opens opportunities to control the structure formation of other supramolecular or coordination polymers that contain paramagnetic ions.

Supramolecular polymers consist of monomers held together by reversible non-covalent interactions.[1] Their properties are commonly controlled by external stimuli,[2] such as temperature,[1] enzymes,[3–5] mechanical forces,[6,7] light,[8–10] pH[11–13] or redox potential.[14,15] In addition, external aligning forces due to electric fields, centrifugal gravity or flow have been shown to affect the growth and orientation of supramolecular polymers.[16] When using magnetic fields, large values ~10 T are needed align diamagnetic molecules that contain no paramagnetic atoms or magnetic nanoparticles).

By introducing ferrimagnetic or paramagnetic species, alignment can be obtained at lower fields (mT to T), for example by using magnetite nanocrystals[17], clay particles[18], bicelles[19], or self-assembled dumbells[20]. From an energetic point of view, it must be that many paramagnetic moments act together, when combined into a self-assembled structure. As an indication, in a uniform 1 T field the magnetic energy $U_m = -\frac{1}{2} mB$ of a single paramagnetic Gd^{3+} ion at room temperature, is $-3 \cdot 10^{-25}$ J,[21] four orders of magnitude smaller than the thermal energy at room temperature $E_T = k_B T = 4 \cdot 10^{-21}$ J. The studies described so far have focused on magnetic fields applied during irreversible assembly processes, such as crystallization[22], drying, pH-change[23], cross-diffusion[24] in layered systems or orientation of pre-formed particles[25].

Here, we set out to understand how 1–2 T magnetic fields can perturb equilibrium supramolecular polymers in solution, in a reversible manner. That is, by applying the magnetic field we perturb the thermodynamic equilibrium, and reach a new magnetically-induced equilibrium. We will show that whereas single polymer rods are not affected by the magnetic field, networks of rods are. Overall, the mass contained in the rod assemblies increases in presence of the magnetic field. Removal of the field causes the system to relax back to its original thermodynamic equilibrium.

Specifically, we use a previously studied C_3-symmetrical benzene-1,3,5-tricarboxamide BTA derivative, extended by fluorinated *L*-phenylalanine and connected to 1,4,7,10-tetraazacyclododecane-N,N',N'',N'''-tetraacetic acid (DOTA) groups[26] (see also the work on closely related derivatives[27–29]). The latter molecule will be called Gd-BTA when chelated to gadolinium(III), or Y-BTA when chelated to yttrium(III) as a negative diamagnetic control (Fig. 1a,b). Previously, it was shown that Gd-BTA assembles into supramolecular rods using a cooperative (nucleation/elongation) polymerization mechanism, with dimensionless nucleation constant

K_{nuc} = 10^{-4} and K_e = 1.4 x 10^{-6} M^{-1}.[26] At 100 μM Gd-BTA concentration in 100 mM citrate buffer, as in the current work, there was no sign of macroscopic gelation or changes in viscosity, as compared to buffer alone.

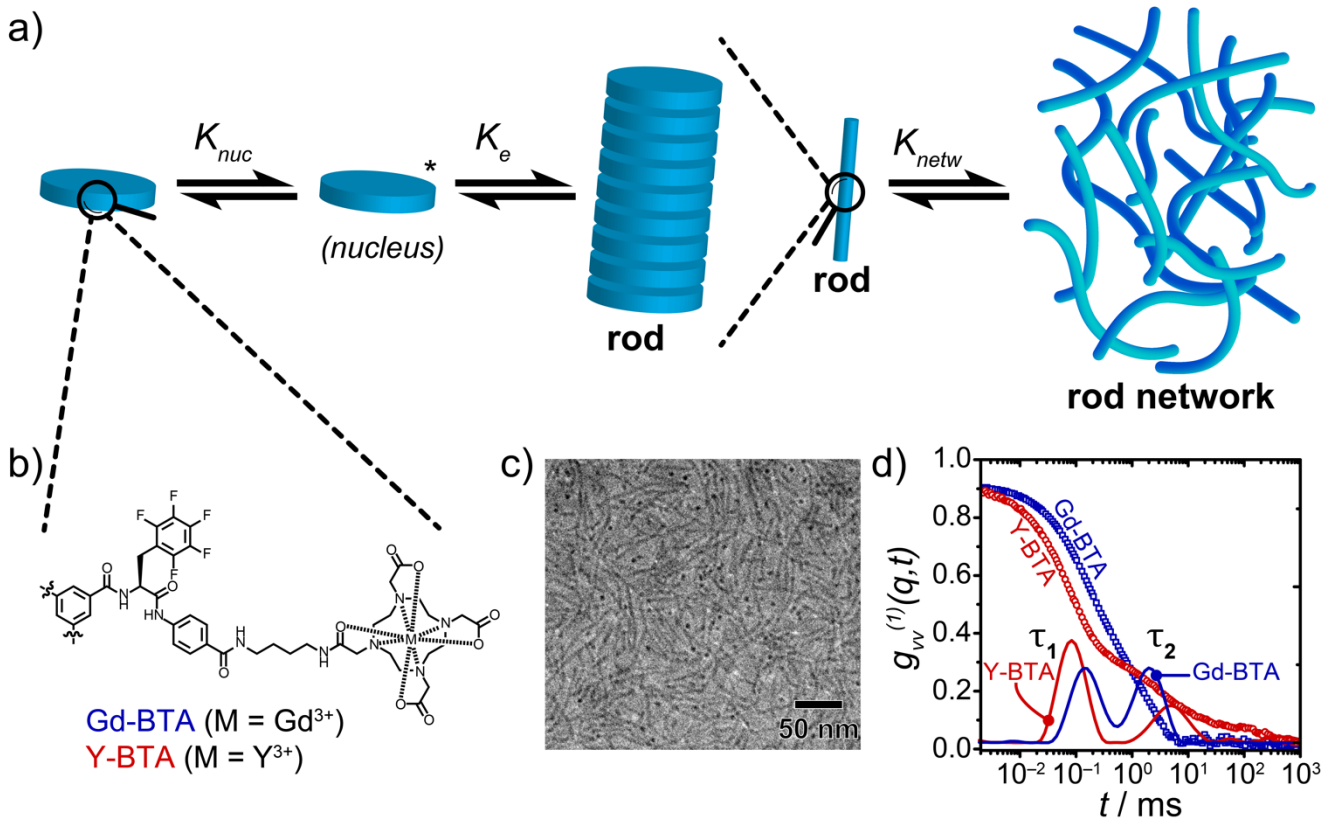

Figure 1. The formation and analysis of rod networks, consisting of supramolecular rods. a) Scheme depicting nucleation K_{nuc} (10^{-4}), elongation K_e (1.4 x 10^6 M^{-1}) and solution network formation K_{netw}. b) Molecular structures of Gd-BTA and Y-BTA. Only 1 out of three arms is shown for compactness. c) Polarized field correlation function $g_{VV}^{(1)}(q,t)$ at 100 μM concentration in 100 mM citrate buffer at pH 6 measured at q = 0.0288 nm^{-1}, shown by the hollow symbols. The solid lines show the corresponding bimodal distribution of relaxation times. d) Cryo-transmission electron microscopy image of the rods and rod networks formed by Gd-BTA at 100 μM in 100 mM Citrate (pH = 6). The scale bar is 50 nm.

In the current work, we show that the rods assemble further into rod networks (simplistically represented by K_{netw} in Fig. 1a), as can be seen from cryo-TEM in Figure 1c. The rods and rod networks can also be measured in their native solution state, using dynamic light scattering. Figure 1d shows the vertical–vertical (vv) polarized electric field autocorrelation function $g_{VV}^{(1)}(q,t)$ at a scattering wavevector q = 0.0288 nm^{-1}, which shows a decay versus time shift t. The latter function can be used to extract a distribution of relaxation times τ (solid lines in Figure 1d) by using the inverse Laplace transformation.[30] Starting with Gd-BTA (blue line), we can see that there are two distinct relaxation processes with typical timescales $\tau_{1,Gd\text{-}BTA}$ and $\tau_{2,Gd\text{-}BTA}$, corresponding to rods and rod networks, respectively, that differ by more than an order of magnitude. Both processes are q^2-dependent and are thus diffusive, allowing us to fit their diffusion constants $D_H = \Gamma.q^{-2}$ (where Γ is the decay constant), and convert the latter into hydrodynamic radii using the Stokes–Einstein equation $R_H = k_B T/6\pi\eta D_H$ (where η is the dynamic viscosity). Table 1 shows the hydrodynamic radii for both Gd-BTA and Y-BTA samples. We can convert the values of $R_{H,1}$ into rod lengths using the Tirado[31] model (with a fixed radius of 3.1 nm deduced from cryo-TEM, Figure 1c). This results in rod lengths in solution of ~245 nm for Gd-BTA and ~120 nm for Y-BTA

(see Table 1, middle column). Though in a prior study[26] we had shown that Y(III) was a good control ion—that is, having identical assembly behavior and sizes as compared to its Gd(III) analog—in this case, the Gd-BTA rods are twice as long as those of Y-BTA (cf. Table 1). Yttrium is often 8-coordinated, whereas gadolinium can be 8 or 9-coordinate, which could manifest itself as having one or two coordinated H_2O molecules at the Gd atom in solution, respectively. Since we have other control experiments—i.e., Gd-BTA in absence of the magnetic field—we disregard the rod size difference between Y-BTA and Gd-BTA for now.

Table 1. Results from light scattering experiments. Hydrodynamic radii R_H of rods and the rod network from dynamic light scattering (Figure 1d) and the respective rod lengths fit to the Tirado model.[31]

Species	*Rods:* $R_{H,1}$ (nm)	Rod length from $R_{H,1}$ (nm)	*Rod network:* $R_{H,2}$ (nm)
Gd-BTA	30.5 ± 4.5	245 (calc.)	348.2 ± 69
Y-BTA	17.9 ± 1.5	120 (calc.)	503.7 ± 169.6

The structure of the rod networks can be studied in more detail by static light scattering, where the Rayleigh ratio has a power law dependency $R(q) \propto q^{-d_F}$ (Fig. 2a), with d_F the fractal dimension. In general, $d_F = 1$ (one-dimensional) describes a line, and the upper limit $d_F = 3$ (three-dimensional) a sphere.[32] In the absence of a magnetic field we find d_F of our rod network to be 1.7 ± 0.2, in agreement with literature[33,34]. The d_F value was independently confirmed by box-counting cryo-TEM images of Gd-BTA, with values of 1.77–1.85 (see SI Section 2). In the experiments that follow we use d_F to quantify the rod network *topology*, and the Rayleigh ratio $R(q)$ to determine the approximate *mass* contained in the network.

Practically, a light scattering cuvette was placed between the pole pieces of an electromagnet for 1 h, then analyzed by light scattering (~1 h) without field, and placed back in the magnetic field. This cycle was repeated 6–7 times (12–14 h in total). Within the first hour, the fractal dimension d_F changes from 1.7 ± 0.2 to 2.2 ± 0.2 (1 T) or 2.6 ± 0.2 (2 T) and then remains constant for the rest of the experiment (see Fig. S1 in the SI). This implies that the increased magnetic field leads to an increasingly dense network structure, ending up at 2 T with randomly branched clusters.[35–37] In contrast, the $R(q)$ for the Gd-BTA rod network keeps on increasing gradually over time, and reaches a plateau only after 10–12 h. The final plateau values are 20% (1 T) or 35% (2 T) higher than the original value, in no field. The latter shows that more rods are contained in the rod network, pointing at an increase in K_{netw} upon applying the magnetic field, as we will discuss below. After removal of the magnetic field, the samples returned to their original *R(q)* values within one day.

Surprisingly, the individual rods (open symbols, Fig. 2b) are not detectably affected by the magnetic field, since their *R(q)* remains constant. If the sample is not exposed to the magnetic field, the value of $R(q)$ for the network remains constant as well (see grey dashed box in Fig. 2b). Likewise, for weakly diamagnetic Y-BTA, no changes were observed.

Our qualitative interpretation thus far is that the network topology changes fast (< 1 hour), and this slowly drives additional rods to assemble into rod networks, taking ~12 hours as evidenced by the increase in Rayleigh scattering *R(q)* intensity. It is known that isodesmic supramolecular polymers elongate in aligning fields (including electric fields, flow fields, or gravitational/centrifugal fields).[16] In the latter case, the field (partially) aligns the polymer which entropically favors the polymer to elongate. The latter in turn increases the degree of

alignment of the polymer as it is now longer, and it provides positive feedback. Analogously, we believe that the magnetic field entropically favors rods to assemble increasingly into rod networks.

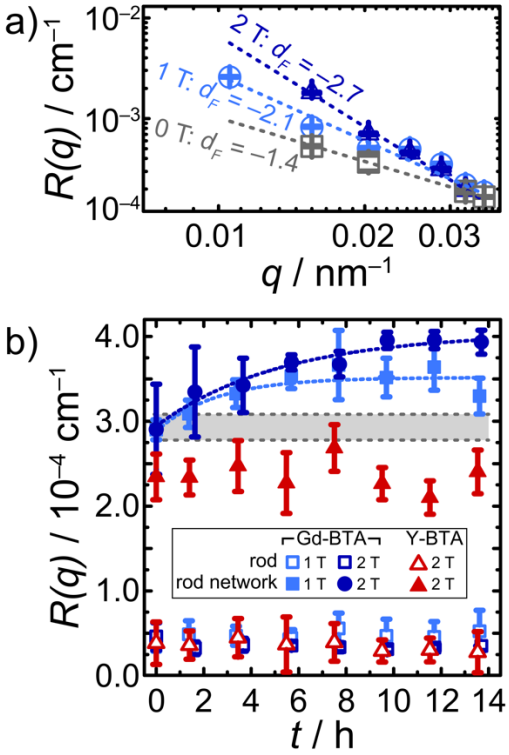

Figure 2. Quantification of rod network topologies upon exposure to magnetic fields. a) Rayleigh ratio *R(q)* of Gd-BTA rod networks as a function of wavevector *q* at 0, 1 or 2 T applied magnetic field. The slopes of the curves give the fractal dimension d_F (values shown in the graph). Error bars are standard deviations calculated over 5 measurements. b) Rayleigh ratio *R(q) at q* = 0.0288 nm^{-1} over time for rods and rod networks, denoted by hollow and filled symbols, respectively. The gray area represents the control for Gd-BTA in absence of a magnetic field (mean and standard deviation). Error bars show standard deviations over 50 measurements.

To come to a more quantitative understanding we have compared the magnetic properties of Gd-BTA and Y-BTA. We first checked for interactions between the Gd^{3+} ions by measuring the susceptibility χ versus temperature in a SQUID (superconducting quantum interference device) magnetometer. The data in Fig. 3a) show Curie–Weiss behavior $\chi = C(T - \theta)$ with a very small negative paramagnetic Curie temperature of $\theta = -0.7$ K. Such weak antiferromagnetic coupling between the Gd^{3+} ions in the rods is negligible at room temperature, and it cannot explain our observed field effect on the rod network (Fig. 2b). We also subjected samples to a constant 5 T field for up to 12 h while monitoring the magnetic susceptibility. For Gd-BTA, the susceptibility decreased by ~2% with respect to the original value χ_0 on a timescale commensurate with that found in the light scattering experiments (Fig. 3b). The latter results indicate a minor alignment of the rods in the network upon exposure to the magnetic field. By optical birefringence in our light scattering setup, however, no changes could be observed at 1 or 2 T. As expected, changes were not observed in the case of Y-BTA or a buffer solution.

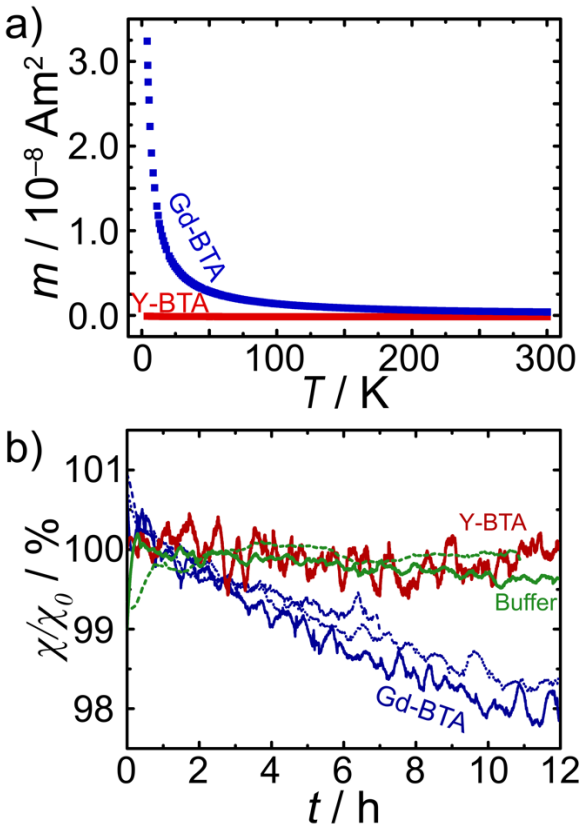

Figure 3. Magnetic characterization of supramolecular rods and rod networks. a) Temperature-dependent magnetization curve of Gd-BTA and Y-BTA in powder form, blue and red respectively. *m* represents the magnetization of the sample in A m^2. Gd-BTA shows a weak antiferromagnetic coupling of –0.7 K while the Y-BTA molecule showed no paramagnetism. b) Room-temperature time-dependent magnetization of Gd-BTA and Y-BTA (blue and red lines respectively) in solution, and as a negative control the buffer separately (in green). The samples were place in the SQUID under 5 T magnetic field and their magnetization was measured over the course of 12 h. The solid and dotted lines are separate experiments. The increase of the demagnetizing factor of the Gd-BTA with time is due to the evolution of the supramolecular structure.

Let us now consider how the magnetic field could affect the network structure. Under normal conditions the distribution of rods versus rod networks is governed by an equilibrium constant, K_{netw} as seen in Fig. 1a. This is a simplified representation, since a single equilibrium constant does not consider the length and distribution of the rods. Keeping that in mind, we can express K_{netw} as:

$$K_{netw} = e^{-\frac{\Delta G_0 + \Delta G_m}{RT}}$$

where ΔG_0 is the Gibbs free energy at 298 K and 0 T. The additional term, ΔG_m, is a magnetic Gibbs free energy induced by the magnetic field, which has two components: 1) an isotropic term $U_i = -\frac{1}{2} MB$ stemming from the isotropic sum of all individual Gd^{3+} ion contributions (see supporting information section 3), and 2) an anisotropic free energy is defined as:[21]

$$U_a = \frac{1}{4}\,\mu_0\, M_s^2\,(1 - 3N)$$

with N the effective demagnetizing factor ($N = 0$ for an axially magnetized long rod), M_s the induced magnetization and μ_0 the vacuum permeability. For our rods with M_s = 600 A m^{-1} (see section 3 of the SI), the

anisotropy energy is therefore 0.17 J m^{-3}. The volume V of a supramolecular network that can have its structure modified by the applied field can be estimated by setting $U_a V = kT$, which gives $V = 24 \cdot 10^{-21}$ m^3, or a size of about 300 nm.

In conclusion, we have shown pronounced changes in the network structure of supramolecular polymer rods containing paramagnetic ions on applying magnetic fields of 1–2 T. The magnetic free energy contributions are insignificant at the single rod level, but they become significant at the network scale. It is the magnetic dipole anisotropy energy that drives the network changes. Our approach could guide structure formation of other supramolecular and coordination polymers using rare earth or other paramagnetic ions.

ASSOCIATED CONTENT

Supporting Information

AUTHOR INFORMATION

Corresponding Author

Thomas M. Hermans – Université de Strasbourg, CNRS, UMR7140, Strasbourg, France; orcid.org/0000-0003-1121-1754; Email: hermans@unistra.fr

Authors

Vincent Marichez – Université de Strasbourg, CNRS, UMR7140, Strasbourg, France

Akihiro Sato – Université de Strasbourg, CNRS, UMR7140, Strasbourg, France

Peter Dunne – Université de Strasbourg, CNRS, UMR7140, Strasbourg, France

Jorge Leira-Iglesias – Université de Strasbourg, CNRS, UMR7140, Strasbourg, France

Georges J. M. Formon – Université de Strasbourg, CNRS, UMR7140, Strasbourg, France

Michaela K. Schicho – Université de Strasbourg, CNRS, UMR7140, Strasbourg, France

Isja de Feijter – Laboratory of Macromolecular and Organic Chemistry, Eindhoven University of Technology, Eindhoven 5600 MB, The Netherlands

E. W. Meijer – Laboratory of Macromolecular and Organic Chemistry, Eindhoven University of Technology, Eindhoven 5600 MB, The Netherlands

Pascal Hébraud – Institut de Physique et Chimie des Materiaux de Strasbourg, UMR 7504 CNRS-Université de Strasbourg, 23 rue du Loess, 67034 Strasbourg, France

Matthieu Bailleul – Institut de Physique et Chimie des Materiaux de Strasbourg, UMR 7504 CNRS-Université de Strasbourg, 23 rue du Loess, 67034 Strasbourg, France

Pol Besenius – Department of Chemistry, Johannes Gutenberg-University Mainz, Duesbergweg 10–14, 55128 Mainz, Germany

M. Venkatesan – School of Physics, Trinity College, Dublin 2, Ireland

J.M.D. Coey – School of Physics, Trinity College, Dublin 2, Ireland

Notes

The authors declare no competing financial interest.

ACKNOWLEDGEMENTS

VM, AS, JLI, and TMH would like to acknowledge the funding from ANR-10-LABX-0026 CSC. GJMF received funding from Ministère de l'Education Nationale de l'Enseignement supérieur et de la Recherche. EWM acknowledges funding of the Dutch Ministry of Education, Culture and Science (Gravitation program 024.001.035). PD and TMH acknowledge the support of the Labex NIE 11-LABX-0058_NIE within the Investissement d'Avenir program ANR-10-IDEX-0002-02, the support of the University of Strasbourg Institute for Advanced Studies (USIAS) Fellowship. PD acknowledges support from SALTYSPIN ANR-17-CE09-0005. MV was funded by Science Foundation Ireland grant 16/IA/ 4534 ZEMS. JMDC acknowledges a Gutenberg visiting professorship from the University of Strasbourg

REFERENCES

(1) Aida, T.; Meijer, E. W. Supramolecular Polymers – We've Come Full Circle. *Israel Journal of Chemistry* **2020**, *60* (1–2), 33–47. https://doi.org/10.1002/ijch.201900165.

(2) Aida, T.; Meijer, E. W.; Stupp, S. I. Functional Supramolecular Polymers. *Science* **2012**, *335* (6070), 813–817. https://doi.org/10.1126/science.1205962.

(3) Hirst, A. R.; Roy, S.; Arora, M.; Das, A. K.; Hodson, N.; Murray, P.; Marshall, S.; Javid, N.; Sefcik, J.; Boekhoven, J.; Van Esch, J. H.; Santabarbara, S.; Hunt, N. T.; Ulijn, V. R. Biocatalytic Induction of Supramolecular Order. *Nature Chemistry* **2010**, *2* (12), 1089–1094. https://doi.org/10.1038/nchem.861.

(4) Webber, M. J.; Newcomb, C. J.; Stupp, S. I. Switching of Self-Assembly in a Peptide Nanostructure with a Specific Enzyme. *Soft Matter* **2011**, *7* (20), 9665–9672. https://doi.org/10.1039/c1sm05610g.

(5) Sorrenti, A.; Leira-Iglesias, J.; Sato, A.; Hermans, T. M. Non-Equilibrium Steady States in Supramolecular Polymerization. *Nature Communications* **2017**, *8* (May), 15899. https://doi.org/10.1038/ncomms15899.

(6) Carnall, J. M. A.; Waudby, C. A.; Belenguer, A. M.; Stuart, M. C. A.; Peyralans, J. J. P.; Otto, S. Mechanosensitive Self-Replication Driven by Self-Organization. *Science* **2010**, *327*, 1502–1507.

(7) Herpt, V. J. T.; Stuart, M. C. A.; Browne, W. R.; Feringa, B. L. Mechanically Induced Gel Formation. *Langmuir* **2013**, *29* (28), 8763–8767.

(8) Adhikari, B.; Yamada, Y.; Yamauchi, M.; Wakita, K.; Lin, X.; Aratsu, K.; Ohba, T.; Karatsu, T.; Hollamby, M. J.; Shimizu, N.; Takagi, H.; Haruki, R.; Adachi, S.; Yagai, S. Light-Induced Unfolding and Refolding of Supramolecular Polymer Nanofibres. *Nature Communications* **2017**, *8* (May), ncomms15254. https://doi.org/10.1038/ncomms15254.

(9) Iwaura, R.; Shimizu, T. Reversible Photochemical Conversion of Helicity in Self-Assembled Nanofibers from a 1,ω-Thymidylic Acid Appended Bolaamphiphile. *Angewandte Chemie International Edition* **2006**, *45* (28), 4601–4604. https://doi.org/10.1002/anie.200601173.

(10) Li, L.; Jiang, H.; Messmore, B. W.; Bull, S. R.; Stupp, S. I. A Torsional Strain Mechanism To Tune Pitch in Supramolecular Helices. *Angew. Chem. Int. Ed.* **2007**, *46*, 5873–5876. https://doi.org/10.1002/anie.200701328.

(11) Zhang, J.; Hao, R.; Huang, L.; Yao, J.; Chen, X.; Shao, Z. Self-Assembly of a Peptide Amphiphile Based on Hydrolysed Bombyx Mori Silk Fibroin. *Chemical Communications* **2011**, *47* (37), 10296–10298. https://doi.org/10.1039/c1cc12633d.

(12) Frisch, H.; Unsleber, J. P.; Lüdeker, D.; Peterlechner, M.; Brunklaus, G.; Waller, M.; Besenius, P. PH-Switchable Ampholytic Supramolecular Copolymers. *Angew. Chem. Int. Ed.* **2013**, *52*, 10097–10101. https://doi.org/10.1002/anie.201303810.

(13) Moyer, T. J.; Finbloom, J. A.; Chen, F.; Toft, D. J.; Cryns, V. L.; Stupp, S. I. PH and Amphiphilic Structure Direct Supramolecular Behavior in Biofunctional Assemblies. *J. Am. Chem. Soc.* **2014**, *136* (42), 14746–14752.

(14) Ohta, E.; Sato, H.; Ando, S.; Kosaka, A.; Fukushima, T.; Hashizume, D.; Yamasaki, M.; Hasegawa, K.; Muraoka, A.; Ushiyama, H.; Yamashita, K.; Aida, T. Redox-Responsive Molecular Helices with Highly Condensed p -Clouds. *Nature Chemistry* **2010**, *3* (1), 68–73. https://doi.org/10.1038/nchem.900.

(15) Leira-Iglesias, J.; Sorrenti, A.; Sato, A.; Dunne, P. A.; Hermans, T. M. Supramolecular Pathway Selection of Perylenediimides Mediated by Chemical Fuels. *Chemical Communications* **2016**, *52* (58), 9009–9012. https://doi.org/10.1039/c6cc01192f.

(16) Ciferri, A. *Supramolecular Polymers, Second Edition*; CRC Press, 2005.

(17) Singh, G.; Chan, H.; Baskin, A.; Gelman, E.; Repnin, N.; Král, P.; Klajn, R. Self-Assembly of Magnetite Nanocubes into Helical Superstructures. *Science* **2014**, *345* (6201), 1149–1153. https://doi.org/10.1126/science.1254132.

(18) Michot, L. J.; Bihannic, I.; Maddi, S.; Funari, S. S.; Baravian, C.; Levitz, P.; Davidson, P. Liquid–Crystalline Aqueous Clay Suspensions. *PNAS* **2006**, *103* (44), 16101–16104. https://doi.org/10.1073/pnas.0605201103.

(19) Isabettini, S.; Massabni, S.; Hodzic, A.; Durovic, D.; Kohlbrecher, J.; Ishikawa, T.; Fischer, P.; Windhab, E. J.; Walde, P.; Kuster, S. Molecular Engineering of Lanthanide Ion Chelating Phospholipids Generating Assemblies with a Switched Magnetic Susceptibility. *Phys. Chem. Chem. Phys.* **2017**, *19* (31), 20991–21002. https://doi.org/10.1039/C7CP03994H.
(20) Polarz, S.; Bährle, C.; Landsmann, S.; Klaiber, A. Panoscopic Structures by Hierarchical Cascade Self-Assembly of Inorganic Surfactants with Magnetic Heads Containing Dysprosium Ions. *Angew. Chem. Int. Ed.* **2013**, *52* (51), 13665–13670. https://doi.org/10.1002/anie.201303565.
(21) Coey, J. M. D. *Magnetism and Magnetic Materials*; Cambridge University Press: Cambridge, 2010.
(22) Klara, S. S.; Saboe, P. O.; Sines, I. T.; Babaei, M.; Chiu, P.-L.; DeZorzi, R.; Dayal, K.; Walz, T.; Kumar, M.; Mauter, M. S. Magnetically Directed Two-Dimensional Crystallization of OmpF Membrane Proteins in Block Copolymers. *J. Am. Chem. Soc.* **2016**, *138* (1), 28–31. https://doi.org/10.1021/jacs.5b03320.
(23) Wallace, M.; Cardoso, A. Z.; Frith, W. J.; Iggo, J. A.; Adams, D. J. Magnetically Aligned Supramolecular Hydrogels. *Chem. Eur. J.* **2014**, *20* (50), 16484–16487. https://doi.org/10.1002/chem.201405500.
(24) Radvar, E.; Shi, Y.; Grasso, S.; Edwards-Gayle, C. J. C.; Liu, X.; Mauter, M. S.; Castelletto, V.; Hamley, I. W.; Reece, M. J.; S. Azevedo, H. Magnetic Field-Induced Alignment of Nanofibrous Supramolecular Membranes: A Molecular Design Approach to Create Tissue-like Biomaterials. *ACS Appl. Mater. Interfaces* **2020**. https://doi.org/10.1021/acsami.0c05191.
(25) Matsumoto, K.; Kimura, F.; Tsukui, S.; Kimura, T. X-Ray Diffraction of a Magnetically Oriented Microcrystal Suspension of l-Alanine. *Crystal Growth & Design* **2011**, *11* (4), 945–948. https://doi.org/10.1021/cg200090u.
(26) Besenius, P.; Portale, G.; Bomans, P. H. H.; Janssen, H. M.; Palmans, A. R. A.; Meijer, E. W. Controlling the Growth and Shape of Chiral Supramolecular Polymers in Water. *Proceedings of the National Academy of Sciences* **2010**, *107* (42), 17888–17893. https://doi.org/10.1073/pnas.1009592107.
(27) Besenius, P.; Goedegebure, Y.; Driesse, M.; Koay, M.; Bomans, P. H. H.; Palmans, A. R. A.; Dankers, P. Y. W.; Meijer, E. W. Peptide Functionalised Discotic Amphiphiles and Their Self-Assembly into Supramolecular Nanofibres. *Soft Matter* **2011**, *7* (18), 7980–7983. https://doi.org/10.1039/C1SM05896G.
(28) Schaefer, C.; Voets, I. K.; Palmans, A. R. A.; Meijer, E. W.; van der Schoot, P.; Besenius, P. Controlling the Cooperativity in the Supramolecular Polymerization of Ionic Discotic Amphiphiles via Electrostatic Screening. *ACS Macro Letters* **2012**, *1* (7), 830–833. https://doi.org/10.1021/mz300218e.
(29) Feijter, D. I.; Besenius, P.; Albertazzi, L.; Meijer, E. W.; Palmans, A. R. A.; Voets, I. K. Mechanistic Control over Morphology : Self-Assembly of a Discotic Amphiphile in Water. *Soft Matter* **2013**, *9*, 10025–10030. https://doi.org/10.1039/c3sm52104d.
(30) Provencher, S. W. A Constrained Regularization Method for Inverting Data Represented by Linear Algebraic or Integral Equations. *Computer Physics Communications* **1982**, *27* (3), 213–227. https://doi.org/10.1016/0010-4655(82)90173-4.
(31) Tirado, M. M.; Martínez, C. L.; de la Torre, J. G. Comparison of Theories for the Translational and Rotational Diffusion Coefficients of Rod-like Macromolecules. Application to Short DNA Fragments. *The Journal of Chemical Physics* **1984**, *81* (4), 2047–2052. https://doi.org/10.1063/1.447827.
(32) Raper, J. A.; Amal, R. Measurement of Aggregate Fractal Dimensions Using Static Light Scattering. *Particle & Particle Systems Characterization* **1993**, *10* (5), 239–245. https://doi.org/10.1002/ppsc.19930100505.
(33) Mohraz, A.; Moler, D. B.; Ziff, R. M.; Solomon, M. J. Effect of Monomer Geometry on the Fractal Structure of Colloidal Rod Aggregates. *Physical Review Letters* **2004**, *92* (15), 1555031–1555034. https://doi.org/10.1103/PhysRevLett.92.155503.
(34) Hough, L. A.; Islam, M. F.; Hammouda, B.; Yodh, A. G.; Heiney, P. A. Structure of Semidilute Single-Wall Carbon Nanotube Suspensions and Gels. *Nano Letters* **2006**, *6* (2), 313–317.
(35) Schaefer, D. W. Polymers, Fractals, and Ceramic Materials. *Science* **1989**, *243*, 1023–1027.
(36) Schaefer, D. W.; Brown, J. M.; Anderson, D. P.; Zhao, J.; Chokalingam, K.; Tomlin, D.; Ilavsky, J. Structure and Dispersion of Carbon Nanotubes. In *Journal of Applied Crystallography*; 2003; Vol. 36, pp 553–557. https://doi.org/10.1107/S0021889803005028.
(37) Bauer, B. J.; Hobbie, E. K.; Becker, M. L. Small-Angle Neutron Scattering from Labeled Single-Wall Carbon Nanotubes. *Macromolecules* **2006**, *39*, 2637–2642.